Energy Relaxation Rates in AlInN/AlN/GaN Heterostructures

E. TIRAS,[1,3] S. ARDALI,[1] E. ARSLAN,[2] and E. OZBAY[2]

1.—Department of Physics, Faculty of Science, Anadolu University, Yunus Emre Campus, 26470 Eskisehir, Turkey. 2.—Nanotechnology Research Center, Department of Physics, and Department of Electrical and Electronics Engineering, Bilkent University, 06800 Ankara, Turkey. 3.—e-mail: etiras@anadolu.edu.tr

The two-dimensional (2D) electron energy relaxation in $Al_{0.83}In_{0.17}N/AlN/GaN$ heterostructures has been investigated experimentally. Shubnikov–de Haas (SdH) effect measurements were employed in the investigations. The electron temperature (T_e) of hot electrons was obtained from the lattice temperature (T_L) and the applied electric field dependencies of the amplitude of SdH oscillations. The experimental results for the electron temperature dependence of power loss are also compared with current theoretical models for power loss in 2D semiconductors. The power loss from the electrons was found to be proportional to ($T_e^3 - T_L^3$) for electron temperatures in the range 1.8 K $< T_e <$ 14 K, indicating that the energy relaxation of electrons is due to acoustic phonon emission via unscreened piezoelectric interaction. The effective mass and quantum lifetime of the 2D electrons have been determined from the temperature and magnetic field dependencies of the amplitude of SdH oscillations, respectively. The values obtained for quantum lifetime suggest that remote ionized impurity scattering is the dominant scattering mechanism in $Al_{0.83}In_{0.17}N/AlN/GaN$ heterostructures.

Key words: GaN heterostructure, electron energy relaxation, power loss, phonon emission, Shubnikov–de Haas, Hall mobility

INTRODUCTION

Group III-nitride materials are very suitable for applications in high-power, high-frequency, and high-temperature electronics.[1] Knowledge on fundamental electron transport properties, such as the effective mass of two-dimensional (2D) electrons and relaxation times, is important for exploration and optimization of this material system for device applications. Device performance under high electric field is also important for these systems. At high electric field, the electrons equilibrate at much higher temperature than the lattice temperature. Therefore, determination of the temperature of those hot electrons is of technological and fundamental importance.

The energy relaxation of hot carriers in semiconductors via electron–phonon interaction has been investigated extensively, both experimentally and theoretically, in bulk and two-dimensional 2D structures (for review see Refs. 2–4). The determination of the temperature of electrons, under electric field heating conditions in the steady state, provides useful information about the electron–phonon interactions involved in the energy relaxation process. Since, at temperatures below approximately 30 K to 40 K, the population of optical phonons is negligibly small, acoustic phonon scattering provides the only inelastic scattering mechanism.[4–7]

There are four experimental techniques that have been widely employed, successfully, in investigations of electron relaxation. First, in heavily modulation-doped structures where a highly degenerate electron gas exists, the variation of the amplitude of quantum oscillations, such as in the Shubnikov–de Haas (SdH) effect, with the applied field and lattice temperature can be used in the determination of the electron temperature–power loss characteristics.[3,8,9] Second, in a material where the momentum relaxation is dominated by ionized impurity, remote impurity, interface

roughness, or optical phonon scattering ,[8–11] electron temperatures can be determined as a function of the applied electric field by a simple comparison of the electric field-dependent and lattice temperature-dependent mobility curves.[8–10,12,13] Third, using the noise technique, the electron temperature can be estimated by measuring the electromagnetic radiation results of fluctuations in the electron velocities under high electric field.[14,15] Fourth, with the pump–probe Raman spectroscopy technique, the energy relaxation time can be directly determined from the decay of the anti-Stokes line intensity.[16]

Electron energy relaxation rates in GaN-based samples have been investigated using the different techniques described above.[12–20] In GaN-based heterostructures, a two-dimensional electron gas (2DEG) is formed at the GaN side of the interface between the barrier and GaN layers. Insertion of a thin AlN spacer layer between the barrier and GaN layers helps to increase electron mobility.[21–23]

In-depth understanding of the fundamental optical and electronic properties is yet to be established for the design and development of functional devices. Determination of the temperature of electrons, under electric field heating conditions in the steady state, provides useful information about the electron–phonon interactions involved in the energy relaxation process.[2,5] Furthermore, electron–phonon scattering processes determine the high-field transport phenomena in semiconductors and thus form the basis for many ultrafast electronic and optoelectronic devices. The field of hot carriers in semiconductors thus provides a link between fundamental semiconductor physics and high-speed devices.[24] Despite the fact that the energy relaxation time is a scientifically, technologically, and fundamentally important parameter for designing optoelectronic devices, it is not yet well known. In this work, the temperature of hot electrons (T_e) of the sample and the corresponding power loss (P) have been determined as a function of the applied electric field using the SdH effect method in $Al_{0.83}In_{0.17}$N/AlN/GaN heterostructures. The experimental results determined from SdH measurements are also compared with a two-dimensional model in the acoustic phonon regime. The results are discussed in the framework of current theoretical models concerning carrier energy loss rates in dilute semiconductors.

THEORETICAL BACKGROUND

Magnetotransport measurements have been extensively used in investigations of the electronic transport properties of 2D structures at low temperature. SdH oscillations in the magnetoresistance provide an accurate and sensitive technique that has been employed successfully in investigations of electron energy relaxation in the acoustic phonon regime.[3,25,26] In heavily modulation-doped structures, where a highly degenerate electron gas exists,

Table I. Electronic transport properties of the AlInN/AlN/GaN heterojunction determined at 1.8 K

Parameter	Value
2D carrier density, N_{2D} (10^{16} m^{-2})	7.25
Sheet carrier density, N_H (10^{16} m^{-2})	11.88
Effective mass, m^* (m_0)	0.188
Fermi energy, $E_F - E_1$ (meV)	92.26
Hall mobility, μ_H (cm^2 V^{-1} s^{-1})	6858
Transport mobility, μ_t (cm^2 V^{-1} s^{-1})	7820
Parallel channel mobility, μ_B (cm^2 V^{-1} s^{-1})	3800
Transport lifetime, τ_{tr} (10^{-12} s)	0.836
Quantum lifetime, τ_q (10^{-12} s)	0.264
Lifetime ratio, τ_{tr}/τ_q	3.2
γ	3.55
A (eV s^{-1} K$^{-\gamma}$)	2.9

variations of the amplitude of the SdH oscillations with applied electric field and lattice temperature can be used in the determination of the power loss–electron temperature characteristics. The sample used in the present study is highly degenerate, so that the reduced Fermi energy $\eta = (E_F - E_1)/k_BT \gg 1$ (Table I), even at electron temperatures of approximately 30 K, which is well above the range of temperatures considered here. Therefore, we employed the SdH oscillations technique in our investigations. The method is based on the assumption that ionized impurity scattering, alloy scattering, and interface roughness scattering, which determine the low-temperature transport mobility of electrons, are elastic in nature. Consequently, the energy that is gained by electrons in an applied electric field is dissipated via emission of acoustic phonons.[2,5–7,23,27–32]

The SdH oscillations in the magnetoresistance of a 2D electron gas of single-subband occupancy are well described by the analytical function[33,34]

$$\frac{\Delta\rho_{xx}}{\rho_0} \propto D(\chi) \exp\left(\frac{-\pi}{\omega_c\tau_q}\right) \cos\left[\frac{2\pi(E_F - E_1)}{\hbar\omega_c} - \pi\right], \quad (1)$$

where $\Delta\rho_{xx}, \rho_0, E_F, E_1, \omega_c(= eB/m^*), \tau_q$, and $\hbar$ are the oscillatory magnetoresistivity, zero-magnetic-field resistivity, Fermi energy, first subband energy, cyclotron frequency, quantum lifetime, and Planck's constant, respectively. The exponential term, $\exp(-\pi/\omega_c\tau_q)$, describes the damping due to the collision broadening of the Landau levels. The temperature dependence of the envelope function of the SdH oscillations is totally contained in the term

$$D(\chi) = \frac{\chi}{\sinh\chi} \quad (2)$$

with

$$\chi = \frac{2\pi^2 k_B T}{\hbar\omega_c},$$

where k_B is the Boltzmann constant. The 2D carrier density (N_{2D}) can be calculated[25] using the arguments of Eq. (1)

$$\triangle\left(\frac{1}{B}\right) = \frac{e}{\pi\hbar N_{2D}} = \frac{e\hbar}{m^*(E_F - E_1)}. \quad (3)$$

The thermal damping of the amplitude of the SdH oscillations is, therefore, determined by the temperature, magnetic field, and effective mass via

$$\frac{A(T, B_n)}{A(T_0, B_n)} = \frac{T \sinh(2\pi^2 k_B T_0 m^*/\hbar e B_n)}{T_0 \sinh(2\pi^2 k_B T m^*/\hbar e B_n)}, \quad (4)$$

where $A(T, B_n)$ and $A(T_0, B_n)$ are the amplitudes of the oscillation peaks observed at magnetic field B_n and temperatures T and T_0. In the derivation of Eq. (4) from Eq. (1) it has been assumed that the quantum lifetime (τ_q) is independent of both the temperature and the magnetic field. The quantum lifetime can be determined from the magnetic field dependence of the amplitude of the SdH oscillations (i.e., Dingle plots) at constant temperature provided that the electron effective mass is known[25,26,35]

$$\ln\left[\frac{A(T, B_n) \cdot B_n^{-1/2} \cdot \sinh(\chi)}{\chi}\right] = C - \frac{\pi m^*}{e\tau_q}\frac{1}{B_n}, \quad (5)$$

where C is a constant.

At low temperatures, the contribution to the energy relaxation rates by elastic scattering mechanisms, such as ionized impurity scattering, alloy disorder scattering, and interface roughness scattering, can be neglected.[2] Therefore, inelastic scattering mechanisms should be considered in order to explain the rise of temperature of the 2D electron gas where the applied electric field causes the heating of electrons. Typically, at temperatures below 30 K, longitudinal optical phonon scattering becomes negligible and the main source of energy relaxation is acoustic phonon scattering. Scattering from acoustic phonons includes two independent processes: deformation potential (nonpolar acoustic) scattering and piezoelectric (polar acoustic) scattering. At low temperatures, the carrier distribution is often degenerate, and Pauli exclusion is important in limiting the scattering that is allowed.[2,5–7,28–30] In the 2D calculations, the scattering by the absorption of acoustic phonons was neglected and only spontaneous emission was considered to be important, the infinite-well approximation was used in the extreme quantum limit, and the phonons were assumed to be bulk phonons.[2,3]

The power loss from a degenerate electron gas due to scattering by acoustic phonons has been calculated in two temperature regimes[2,6,7,29]: (i) the low-temperature regime, where the electron temperature $T_e \ll T_e^c$, and (ii) the high-temperature regime, where $T_e \gg T_e^c$, hence the critical electron temperature is given[29] by

$$T_e^c = \frac{\left[8m^*V_S^2(E_F - E_1)\right]^{1/2}}{k_B}, \quad (6)$$

where V_S is the sound velocity. The regime between these two temperature limits is called the intermediate regime.[2,3]

In the low-temperature (Bloch–Grüneisen) regime $(\hbar\omega_q/k_B T_e \gg 1))$ the phonon distribution is given[3] by

$$n(\omega_q) = \frac{1}{\exp(\hbar\omega_q/k_B T_L) - 1} \cong \exp\left(-\frac{\hbar\omega_q}{k_B T_L}\right), \quad (7)$$

where $\hbar\omega_q$ is the acoustic phonon energy at wavevector $\mathbf{q}$. At low temperatures, the Fermi gas has a sharp boundary curve, and consequently momentum changes that involve the emission of an acoustic phonon of energy much greater than $k_B T_e$ are hindered greatly by Pauli exclusion, and hence only small-angle scattering is allowed at very low temperatures.[28,36] Then, in the case under discussion, low-angle scattering should occur in the first subband, which is characterized by the dependencies $P_{np} \propto (T_e^5 - T_L^5)$ for deformation potential scattering and $P_{np} \propto (T_e^3 - T_L^3)$ for piezoelectric scattering.[28,29] Therefore, the total energy loss rate of a 2D electron gas, $P = P_{np} + P_p$, in the low-temperature regime, can be represented[2,3] by

$$P = C_{np}\left[(k_B T_e)^5 - (k_B T_L)^5\right] + C_p\left[(k_B T_e)^3 - (k_B T_L)^3\right], \quad (8)$$

where

$$C_{np} = \frac{6\Xi^2 m^{*2}L_z}{\pi^3 \rho \hbar^7 V_S^4 N_{2D}} \quad (9)$$

and

$$C_p = \frac{e^2 K_{av}^2 m^{*2}}{2\pi^2 \epsilon_s \hbar^5 k_F N_{2D}}; \quad (10)$$

are the magnitudes of the deformation potential and piezoelectric interactions, respectively. Here, Ξ is the acoustic deformation potential, ρ is the mass density, ϵ_s is the static permittivity, and $k_F = [2\pi N_{2D}]^{1/2}$ is the Fermi wavevector of 2D electrons in which N_{2D} is the 2D carrier density. The average electromechanical coupling constant K_{av}^2 for cubic crystal is given[3] by

$$K_{av}^2 = \frac{e_{14}^2}{\epsilon_s}\left[\frac{12}{35C_L} + \frac{16}{35C_T}\right]. \quad (11)$$

Here, e_{14} is the piezoelectric stress constant, and C_L and C_T are the average longitudinal and transverse elastic constants, given[37] in terms of the components of the elastic stiffness constants C_{ij} by

$$C_L = C_{11} + \frac{2}{5}(C_{12} + C_{44} - C_{11}) \quad (12)$$

and

$$C_{\mathrm{T}} = C_{44} - \frac{1}{5}(C_{12} + 2C_{44} - C_{11}). \qquad (13)$$

The screening of the electron–phonon interaction in the 2D case, which is not included in the above calculations, is predicted to increase the exponent of the $k_{\mathrm{B}}T_e$ and $k_{\mathrm{B}}T_{\mathrm{L}}$ terms in Eq. (8) by two.[2,5]

We assumed that the effective well width (L_z) of the potential well at the $\mathrm{Al}_{0.83}\mathrm{In}_{0.17}\mathrm{N/AlN}$ interface approximately equals the average distance of the electrons from the interface derived for only the lowest subband occupied structures using the Fang–Howard variational wave function[34]

$$L_z \approx z_0 = \left[\frac{9\epsilon_{\mathrm{s}}\hbar^2}{4m^*e^2(N_{\mathrm{depl}} + 11N_{\mathrm{2D}}/32)}\right]^{1/3}, \quad (14)$$

where $N_{\mathrm{depl}} = (2\epsilon_{\mathrm{s}}V_{\mathrm{b}}(N_{\mathrm{D}} - N_{\mathrm{A}})/e)^{1/2}$ is the depletion layer charges per unit area, V_{b} is the conduction-band energy offset, N_{D} is the donor concentration, and N_{A} is the acceptor concentration.

The variation of the power loss per electron with electron temperature has been often approximated by the relationship

$$P = A(T_e^{\gamma} - T_{\mathrm{L0}}^{\gamma}), \qquad (15)$$

where T_{L0} is the lowest lattice temperature and A is a proportionality constant that depends on the elastic moduli of the matrix, the coupling constants, and the 2D carrier density. Theoretical calculations of the acoustic phonon-assisted energy loss rates of hot electrons in a 2D electron gas of single subband occupancy predict $\gamma = 1$ at high temperatures (when Maxwell–Boltzmann statistics is applicable and equipartition is assumed) and $\gamma = 3$ (unscreened piezoelectric scattering), $\gamma = 5$ (unscreened deformation potential and heavily screened piezoelectric scatterings), and $\gamma = 7$ (heavily screened deformation potential scattering) at low temperatures (see, for instance, Refs. [2,28–30,38]).

EXPERIMENTAL PROCEDURES

$\mathrm{Al}_{1-x}\mathrm{In}_x\mathrm{N/AlN/GaN}$ ($x = 0.17$) heterostructures were grown on double-polished 2-inch-diameter sapphire ($\mathrm{Al}_2\mathrm{O}_3$) substrates in a low-pressure met-alorganic chemical vapor deposition (MOCVD) reactor (Aixtron 200/4 HT-S) by using trimethyl-gallium (TMGa), trimethylaluminum (TMAl), and ammonia as Ga, Al, and N precursors, respectively. Prior to the epitaxial growth, $\mathrm{Al}_2\mathrm{O}_3$ substrate was annealed at 1100°C for 10 min in order to remove surface contamination. The buffer structures consisted of a 15-nm-thick, low-temperature (770°C) AlN nucleation layer, and high-temperature (1120°C) 270-nm AlN templates. A 1.16-μm, nominally undoped GaN layer was grown on an AlN template layer at 1060°C, followed by a 1.5-nm-thick high-temperature (1075°C) AlN spike layer.

The AlN barrier layer was used to reduce the alloy disorder scattering by minimizing the wave function penetration from the two-dimensional electron gas (2DEG) channel into the AlInN layer. After deposition of these layers, we used 1-nm AlN (1075°C) and 3-nm GaN (1075°C) between the $\mathrm{Al}_{0.83}\mathrm{In}_{0.17}\mathrm{N}$ barrier layer and the AlN spike layer. The thickness of the $\mathrm{Al}_{0.83}\mathrm{In}_{0.17}\mathrm{N}$ barrier layer was 13 nm, and it was grown at 830°C. Finally, a 2-nm-thick GaN cap layer growth was carried out at temperature of 830°C. After the growth, these parameters were measured for each wafer, using standard characterization techniques, such as transmission electron microscopy (TEM), capacitance–voltage profiling, and high-resolution x-ray analysis.

Measurements of longitudinal resistance along the direction of applied current (R_{xx}) were carried out as functions of: (i) the applied electric field F at fixed lattice temperature T_{L0}, and (ii) lattice temperature T_{L} at a fixed electric field F_0 that was low enough to ensure ohmic conditions and hence to avoid carrier heating. In the experiments, a conventional direct-current (DC) technique in combination with a constant-current source (Keithley 2400) and a nanovoltmeter (Keithley 2182A) in a cryogen-free superconducting magnet system (model J2414; Cryogenics Ltd.) were used. The current (I) flow was in the plane of the electron gas. Steady magnetic fields up to 11 T were applied perpendicular to the plane of the samples and, therefore, to the plane of the 2D electron gas. All measurements were taken in the dark. To check the 2D nature of the electron gas giving rise to the quantum oscillations in magnetoresistance, measurements were also performed as a function of the angle θ between the normal to the plane of the 2D electron gas and the applied magnetic field. It was found that the peak position shifted with a factor of $\cos\theta$ and the oscillations disappeared at $\theta = 90°$. This observation is a characteristic of a 2D electron gas.[25]

For the classical low-magnetic-field temperature-dependent Hall-effect measurements, R_{xx} and the Hall resistance (R_{xy}) were measured as a function of temperature from 1.8 K to 275 K. A static magnetic field ($B = 1$ T) was applied to the sample perpendicular to the current plane. The Hall mobility (μ_{H}) and the sheet carrier density (N_{H}) were obtained using the following equations:

$$R_{xy} = \frac{B}{N_{\mathrm{H}}e}, \qquad (16)$$

$$\mu_{\mathrm{H}} = \frac{L}{N_{\mathrm{H}}eR_{xx}b}, \qquad (17)$$

where b (=0.6 mm) and L (=1 mm) are the width and length of the Hall bar. The applied electric field was also obtained using the longitudinal resistance measured at $B = 0$ T ($R_{xx}(B=0) = 118\Omega$) in the following equation:

$$F = \frac{R_{xx}(B=0)I}{L}. \tag{18}$$

In the applied electric field-dependent magnetoresistance measurements, current was applied along the length of the sample in the range of $I = 100\ \mu A$ to $2000\ \mu A$.

The Raman spectra were obtained at room temperature using a Bruker Optics FT-Raman Scope III system. As an excitation source, a wavelength of 785 nm (1.58 eV) was applied in the sample growth direction (c-axis).

RESULTS AND DISCUSSION

The temperature dependence of the sheet carrier density and Hall mobility in the $Al_{0.83}In_{0.17}N/AlN/GaN$ heterostructure is plotted in Fig. 1. At low temperatures, the sheet carrier density remains practically constant up to temperature of 30 K. At higher temperatures, the sheet carrier density increases monotonically with increasing temperature, possibly due to thermally generated carriers located outside the channel. We note that a decrease in the sheet carrier density has been observed in the temperature range from 30 K to 90 K (Fig. 1). A similar behavior of carrier density with temperature, although less pronounced, was reported previously for modulation-doped $GaAs/Ga_{1-x}Al_xAs$ heterojunctions.[39–41]

The Hall mobility of electrons in the $Al_{0.83}In_{0.17}N/AlN/GaN$ heterostructure increases monotonically with decreasing temperature from room temperature, begins to level off at about 100 K, and saturates at about 30 K (Fig. 1). This behavior reflects the 2D character of the electrons in the channel.[25] In the temperature range below 30 K, the mobilities measured for the sample are essentially independent of temperature. A similar behavior for the variation of Hall mobility with temperature was reported[14] for a lattice-matched AlInN/AlN/GaN sample with a 1-nm spacer layer that helps to

reduce remote alloy scattering and achieve high electron mobility (see, for instance, Refs. 21–23,42).

Figure 2 shows typical examples of the magnetoresistance $R_{xx}(B)$ measured at different temperatures and applied electric fields for $Al_{0.83}In_{0.17}N/AlN/GaN$ heterostructures. SdH oscillations are clearly visible over the magnetic field range between $B = 7$ T and 11 T. No higher harmonics are apparent in the oscillations. It is also evident that the oscillatory effect is superimposed on a monotonically increasing component, which occurs as a result of positive magnetoresistance in the barriers.[3] This may affect the accuracy of the determination of the oscillation amplitude, particularly at elevated temperatures. Stradling and Wood[43] adopted the following method to detect the oscillatory component of the magnetoresistance by removing the monotonic component (R_b). Therefore, we used the negative second derivative of the raw magnetoresistance data with respect to the magnetic field, i.e. $(-\partial^2 R_{xx}/\partial B^2)$.[3,25,26,43,44] The SdH oscillations have also been obtained by subtracting the background magnetoresistance (in the form of a polynomial of second degree) from the raw experimental data $(\Delta R = R_{xx} - R_b)$.[45] The values obtained for effective mass and quantum lifetime from the temperature and magnetic field dependence of the normalized amplitude of the oscillations in

Fig. 2. Experimental results showing the effects of (a) temperature and (b) applied electric field on the magnetoresistance $R_{xx}(B)$ measured for an $Al_{0.83}In_{0.17}N/AlN/GaN$ heterostructure sample.
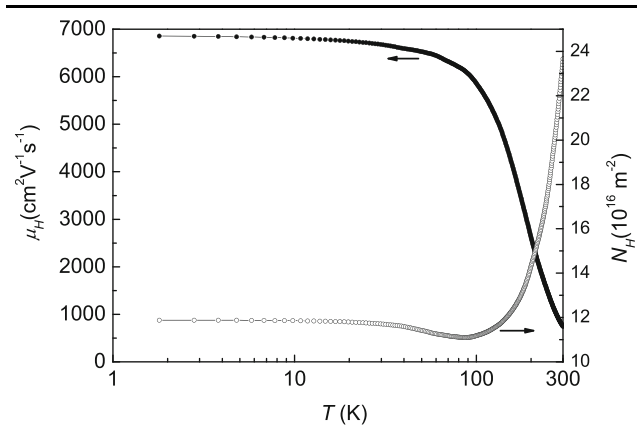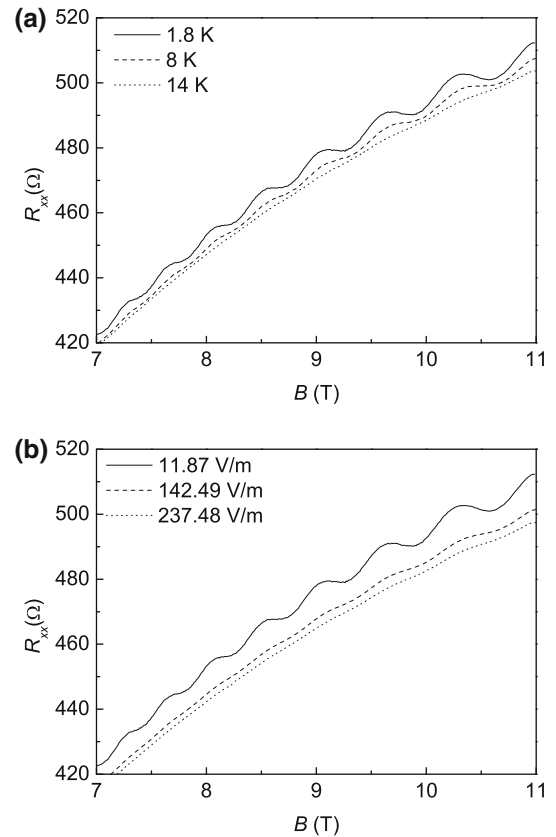

Fig. 1. Temperature dependence of the sheet carrier density (N_H) and Hall mobility (μ_H) of electrons in the $Al_{0.83}In_{0.17}N/AlN/GaN$ heterostructure.
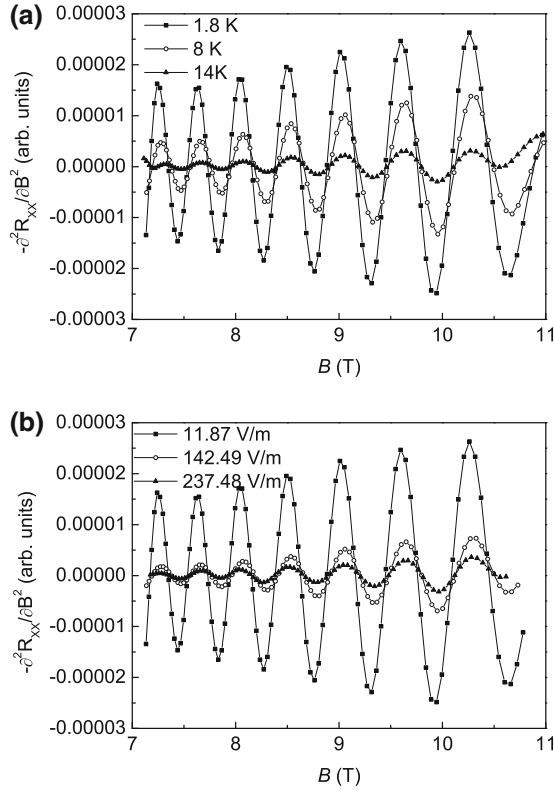
(a)

(b)

Fig. 3. Effects of temperature (a) and applied electric field (b) on the SdH oscillations arising from the electrons in the subband, as extracted from the $R_{xx}(B)$ data for an Al$_{0.83}$In$_{0.17}$N/AlN/GaN heterostructure sample (shown in Fig. 1). The solid curves through the experimental data points are intended as a guide for the eye. The double differentiation removes the background magnetoresistance without affecting the position or amplitude of the oscillatory component.

Fig. 4. The reciprocal magnetic field ($1/B_n$) plotted as a function of the oscillation peak number (n) of Al$_{0.83}$In$_{0.17}$N/AlN/GaN heterostructures measured at 1.8 K. Filled squares correspond to the data given in Fig. 3. The straight line is the least-squares fit to the experimental data. The insert shows the fast Fourier spectrum of the oscillations ($N = 2^8$ and $\Delta T = 4.9 \times 10^{-2}$ T^{-1} is the sampling interval). There is no evidence for population of higher subbands or for any contribution from higher harmonics.

$-\partial^2 R_{xx}/\partial B^2$ agree to within 1% with those found from that of the oscillations in $\Delta R_{xx} = R_{xx} - R_{\mathrm{b}}$. The oscillations in the second derivative of magnetoresistance have well-defined envelopes and are symmetrical about the horizontal line as shown in Fig. 3. The double-differentiation technique does not change the peak position or the period of the oscillations.[25]

The period of the SdH oscillations has been obtained from plots of the reciprocal magnetic field ($1/B_n$), at which the nth peak occurs, against the peak number n. If electrons in only one subband participate in the SdH oscillations, the graph of $1/B_n$ versus n gives a straight line (Fig. 4), the slope of which yields the oscillation period, $\Delta(1/B)$. The Fourier analysis of the SdH oscillations (see the insert in Fig. 4) confirms that only the first subband is populated and that the contribution of higher harmonics is insignificant. The 2D carrier density (N_{2D}) can be calculated using[25] Eq. (3). The oscillation period (and hence the carrier density) that is determined from the SDH oscillation measurements is found to be essentially independent of temperature in the range from 1.8 K to 14 K. The Fermi energies with respect to the subband energy
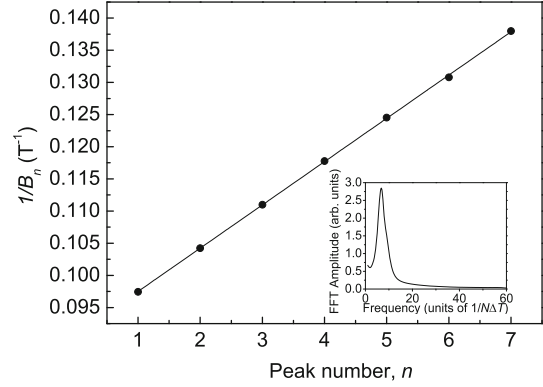
($E_{\mathrm{F}} - E_1$) have been obtained from the oscillation period using Eq. (3) together with the in-plane effective mass m^* of 2D electrons as obtained from the temperature dependence of SdH oscillations (see below). The results found for $E_{\mathrm{F}} - E_1$ are given in Table I.

The 2D carrier density in the Al$_{0.83}$In$_{0.17}$N/AlN/GaN sample determined from the SdH oscillations and the sheet carrier density (N_{H}) obtained from the low-field Hall-effect measurements at 1.8 K are also included in Table I. It can be seen that, within the experimental error owing to the SdH oscillations, the sheet carrier density determined is larger than the carrier density of 2D electrons. This indicates that parallel conduction due to carriers outside the 2D channel is effective for this sample at low temperatures.

The in-plane effective mass of 2D electrons in the Al$_{0.83}$In$_{0.17}$N/AlN/GaN heterostructure can be determined from the temperature dependence of the SdH amplitude at constant magnetic field using Eq. (4). A typical example for the variation of SdH oscillation amplitude with temperature is shown in Fig. 5. The relative amplitude $A(T, B_n)/A(T_0, B_n)$ decreases with increasing temperature in accordance with the usual thermal damping factor [see Eq. (2)]. The in-plane effective mass of 2D electrons determined by fitting the experimental data for the temperature dependence of $A(T, B_n)/A(T_0, B_n)$ to Eq. (4) is also included in Table I. Similar analysis for all the oscillation peaks observed in the magnetic field range from 7 T to 11 T has established that the in-plane effective mass of the 2D electrons is essentially independent of the magnetic field.

Experimentally evaluated electron effective mass in AlGaN/GaN as a function of the two-dimensional electron gas density formed at the interface of an AlGaN/GaN heterostructure with a different alloy
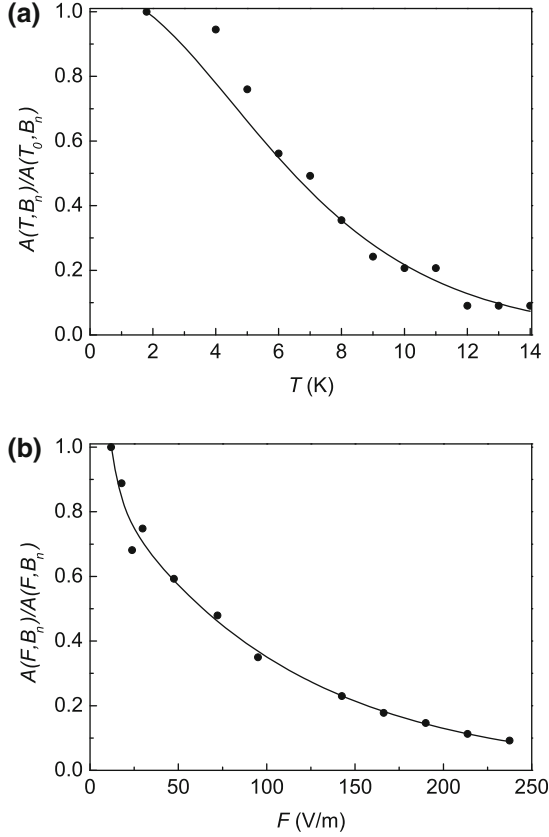
Fig. 5. (a) Temperature and (b) electric field dependencies of the normalized amplitude of the oscillation peak at B_n measured in an Al$_{0.83}$In$_{0.17}$N/AlN/GaN heterostructure. The data points represented by the filled circles correspond to the SdH oscillations arising from the electrons in the first subband. The solid curve in (a) is the best fit of Eq. (4) to the experimental data. The solid curve in (b) is intended as a guide for the eye.

Fig. 6. Determination of the quantum lifetime in the Al$_{0.83}$In$_{0.17}$N/AlN/GaN heterostructure sample. The data points are represented by solid squares, and the straight line is the least-squares fit of Eq. (5) to the experimental data.

composition was summarized by Kurakin et al.[46] They found the electron effective mass in AlGaN/GaN to be independent of the electron concentration. This result for the effective mass of 2D electrons was in good agreement with the bulk effective mass in GaN, which was reported[46,47] to be $0.2 \pm 0.02m_0$ (where m_0 is the free electron mass). The effective mass of 2D electrons in the Al$_{0.83}$In$_{0.17}$N/AlN/GaN heterostructure is in good agreement with the bulk effective mass in GaN.[46,47] This indicates that both the nonparabolicity of the conduction band of GaN and the wave function penetration into the AlN barrier/spacer layer have no significant effects on the effective mass of 2D electrons in our samples.

The SdH oscillations and classical Hall-effect measurements allow for determination of both the quantum and transport lifetimes of the electrons in the Al$_{0.83}$In$_{0.17}$N/AlN/GaN heterostructure and hence to investigate the relative importance of various scattering mechanisms including ionized impurity scattering, alloy scattering, and interface roughness scattering. The quantum lifetime (τ_q) can be determined from the magnetic field dependence
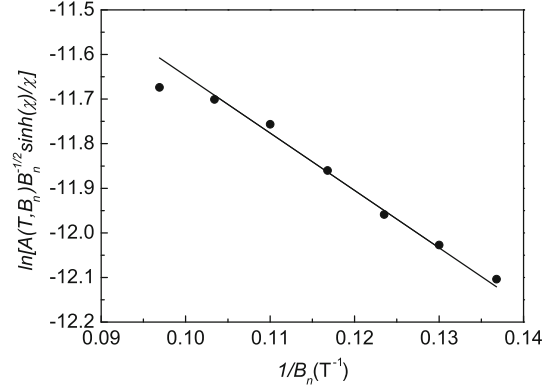
of the amplitude of the SdH oscillations using Eq. (5) together with the measured values of m^* (Table I). Figure 6 shows typical examples of the Dingle plots for the samples investigated. There is good agreement between the experimental data and the straight line described by Eq. (5). The quantum lifetime obtained from the slope of the Dingle plot is also included in Table I. These values remain constant within 2% in the whole temperature and magnetic field ranges of the measurements. The quantum lifetime (τ_q) and quantum mobility (μ_q) are also tabulated together with the transport lifetime (τ_{tr}) and Hall mobility (μ_H) determined using the results of zero-field resistivity and low-field Hall-effect measurements in Table I.

The transport mobilities (μ_t) of the 2D electrons in the quantum well have been calculated using the values (Table I) determined experimentally for the sheet carrier density (N_H), 2D carrier density (N_{2D}), and Hall mobility (μ_H) by following the analysis for parallel conduction by Kane et al.[48] The expressions for the effective Hall mobility and carrier density due to the two conducting channels (quantum well and bulk carriers outside the 2D channel) may be written as

$$N_H = \frac{(N_{2D}\mu_t + N_B\mu_B)^2}{N_{2D}\mu_t^2 + N_B\mu_B^2}, \qquad (19)$$

$$\mu_H = \frac{N_{2D}\mu_t^2 + N_B\mu_B^2}{N_{2D}\mu_t + N_B\mu_B}, \qquad (20)$$

where N_B and μ_B are the electron density and the mobility of the bulk carriers outside the 2D channel. Here, N_B is calculated from the difference between N_H and N_{2D}. The transport mobility (or transport lifetime) of 2D electrons in the Al$_{0.83}$In$_{0.17}$N/AlN/GaN heterostructure sample has been found to be essentially independent of both the lattice temperature in the range from 1.8 K to 14 K and the applied electric field in the range from 11.87 V m^{-1} to 230 V m^{-1}.
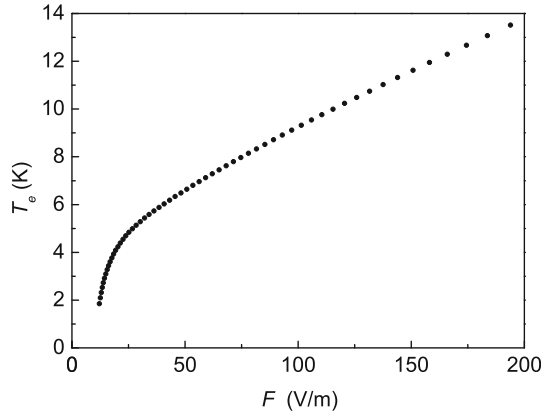
Fig. 7. Electron temperature (T_e) versus applied electric field (F) for $Al_{0.83}In_{0.17}N$/AlN/GaN heterostructures.
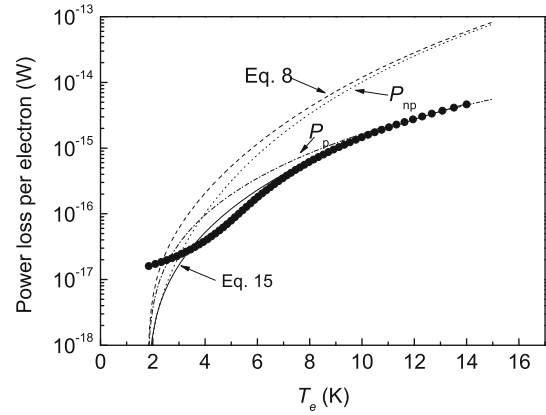

Fig. 8. Electron temperature dependence of power loss per electron determined from SdH measurements. Solid circles correspond to experimental data. Dashed, dotted, dash-dotted, and solid curves correspond to the power loss calculated using Eq. (8), nonpolar component of Eq. (8) (P_{np}), polar component of Eq. (8) (P_p), and Eq. (15), respectively.

The ratio of the quantum to transport lifetime, τ_{tr}/τ_q, in our samples is larger than unity (Table I). Theoretical calculations relating the 2D single-particle scattering time (quantum lifetime) to the momentum relaxation time (transport lifetime) predict a τ_{tr}/τ_q ratio equal to or less than unity for wide-angle scattering and greater than unity for small-angle scattering in the extreme quantum limit for single subband occupancy.[25] This implies that, in our sample, electron scattering with small-angle scattering, such as remote ionized impurity scattering and ionized surface states, is on average forward displaced in momentum space. A similar result is also attributed to AlGaN/GaN heterostructures.[19]

Assuming that the change in the SdH amplitude with applied electric field can be described in terms of electric field-induced electron heating, the temperature T in Eqs. (1–5) can be replaced by the electron temperature T_e.[3,8,9,25] Therefore, T_e can be determined by comparing the relative amplitudes of the SdH oscillations measured as functions of the lattice temperature ($T = T_L$) and the applied electric field (F) using[3,8,9]

$$\left[\frac{A(T_L, B_n)}{A(T_{L0}, B_n)}\right]_{F=F_0} = \left[\frac{A(F, B_n)}{A(F_0, B_n)}\right]_{T_L=T_{L0}}. \quad (21)$$

Here, $A(F, B_n)$ and $A(F_0, B_n)$ are the amplitudes of the oscillation peaks observed at a magnetic field B_n and at electric fields F and F_0, respectively. In order to obtain the electron temperature from the lattice temperature and electric field dependencies of the amplitude of the SdH oscillations, the quantum lifetime has to be independent of both the lattice temperature and the applied electric field. Figure 5b shows the amplitudes of the SdH oscillations, normalized as described by Eq. (18), as functions of F for the $Al_{0.83}In_{0.17}N$/AlN/GaN heterostructure sample. In Fig. 5, only the relative amplitudes at a given magnetic field B_n are shown for clarity. A similar analysis conducted for all the SdH peaks that were observed in the magnetic field range from 7 T to 11 T has established that the relative amplitudes of SdH oscillations (and hence the electron temperatures) in our samples are essentially independent of magnetic field. This indicates that the magnetic field used in our experiments does not significantly alter the energy relaxation processes of hot electrons.

Electron temperatures (T_e) for the $Al_{0.83}In_{0.17}N$/AlN/GaN heterostructure sample as obtained by directly comparing the curves similar to those in Fig. 5a, b are plotted as a function of the applied electric field in Fig. 7. The SdH oscillations measured for the $Al_{0.83}In_{0.17}N$/AlN/GaN heterostructure sample decrease rapidly with increasing applied electric field and become vanishingly small for $F > 230$ V m^{-1} (Figs. 3b, 5b). The electron temperature determined for this sample rises quickly with increasing F.

In the steady state, the power loss from hot electrons by the emission of acoustic phonons is equal to the power supplied by the applied electric field, which can be calculated using the energy balance equation[8,9]

$$P = e\mu_t F^2, \quad (22)$$

where P, μ_t, and F are the energy loss (or energy supply) rate per electron/hole, transport mobility, and applied electric field, respectively. In the calculations of power loss, we used the calculated transport mobilities as given in Table I. The power loss versus electron temperature is plotted in Fig. 8.

Comparing our results determined from SdH measurements with previous reports on energy relaxation of hot electrons in GaN/AlGaN heterojunctions, we find that the magnitude of the power loss determined in this study varies significantly from the power loss given in literature.[17–20] The observed variations in power loss may be associated with the differences in the mobility of the samples,

Table II. Material parameters of the $Al_{0.83}In_{0.17}$N/AlN/GaN heterostructure used in the calculation (Refs. 20,50–52)

Parameter	Value
Ξ (eV)	-7.7
$\varepsilon_S (\varepsilon_0)$	10
C_{11} (GPa)	296
C_{12} (GPa)	141
C_{44} (GPa)	94
e_{14} (C m^{-2})	0.375
ρ (kg m^{-3})	6150
V_S (m/s)	6560
V_b (eV)	1.923
N_D (cm^{-3})	10^{18}

due to its primary role in the calculation of the power loss [see Eq. (21)]. If experimentally determined electron temperature-dependent power loss data are normalized to the mobility, it can be shown that the power loss determined from SdH measurements in literature[17–20] and our results (Fig. 8) match each other rather well.

We found the exponent 3.55 (Table I) by fitting Eq. (15) to the experimental data determined from SdH measurements (Fig. 8). In all cases, a constant value for the exponent γ is obtained over the whole temperature range. This indicates that the experiments were carried out in the low-temperature regime and that the energy relaxation is due to acoustic phonon emission via mixed unscreened piezoelectric and deformation potential interactions.[2,49]

We, therefore, fitted the experimental $P(T_e)$ data, obtained from the measurements at $T_{L0} \approx 1.8$ K, to the analytical expressions for power loss in the low-temperature regime (Fig. 8). The power loss, as given by Eq. (8), was calculated using the values (Table I) determined experimentally for the effective mass, carrier density, and Fermi energy of 2D electrons in the $Al_{0.83}In_{0.17}$N/AlN/GaN heterostructure sample; other parameters were taken from the literature (Table II).[20,50–52]

We attempted to fit the 2D theoretical power loss in the low-temperature regime (Eq. 8) to the experimental $P(T_e)$ results determined from SdH measurements. However, the low-temperature regime model does not offer a satisfactory fit to the experimental data for the $Al_{0.83}In_{0.17}$N/AlN/GaN heterostructure sample. It is also instructive to study the relative magnitude of the deformation potential (nonpolar acoustic) P_{np} and piezoelectric (polar acoustic) P_p components of the electron energy loss rates. In the low-temperature regime, the piezoelectric coupling dominates: $P_{np}/P_p > 1$ for the $Al_{0.83}In_{0.17}$N/AlN/GaN heterostructure sample. These trends remain at all electron temperatures in the range from 1.8 K to 14 K. The polar and nonpolar components of the power loss in the

low-temperature regime are also plotted as a function of electron temperature in Fig. 8. It is evident from Fig. 8 that P_p is in agreement with the experimental power loss data determined above 8 K for the $Al_{0.83}In_{0.17}$N/AlN/GaN heterostructure sample. This result is also in accord with the outcome of fitting Eq. (15) and other researchers' results in AlGaN/GaN heterojunctions.[17–20] To our knowledge, there is no study to date concerning acoustic phonon-assisted energy relaxation of hot electrons in AlInN/AlN/GaN or AlInN/GaN heterostructure samples. Therefore, we have no possibility to compare our experimental results with experimental results from literature.

The dominant process for relaxing the hot electron energy is via the interaction with acoustic phonons below about 100 K and polar optical phonons at 300 K in GaN-based heterostructures.[53,54] The acoustic phonon scattering includes deformation potential scattering and piezoelectric scattering. In view of our experimental observations, we conclude that, in the low-temperature regime, the piezoelectric scattering rates in the 2D case are somewhat overestimated for the $Al_{0.83}In_{0.17}$N/AlN/GaN heterostructure and, hence, the theoretical calculations of the 2D polar interactions need to be reconsidered. From the theoretical calculation, it was shown that in the energy relaxation rates for acoustic phonons the lattice temperature determines the number of excited phonons and the electron temperature affects the screening.[2,53] If screening were to be included in the 2D theoretical calculations for the GaN-based structure, the nonpolar component of the interaction would be reduced significantly for

$$\frac{k}{\sqrt{2m^*\omega_{LO}/\hbar}} < 1, \qquad (23)$$

where k is the electron wavevector and ω_{LO} is the optical phonon frequency,[53] whereas, if screening were to be included in the 2D theoretical calculations for the GaAs-based structure, the polar component of the interaction would be reduced significantly.[2,5,7] Therefore, in order to compare our experimental results with the theoretical results and the calculation using Eq. 23, we used our experimental data to determine the optical phonon energy.

The techniques that are often used to find the optical phonon (LO) energy are Raman or infrared measurements, temperature-dependent Hall mobility measurements, and hot electron power loss measurements. While the first technique gives the LO energy directly from the spectra, the two latter techniques yield this value via use of appropriate energy and momentum relaxation expressions.

In the temperature range above approximately 90 K, where the electron mobility is expected to be limited primarily by polar optical phonon scattering, the temperature dependence of the differential
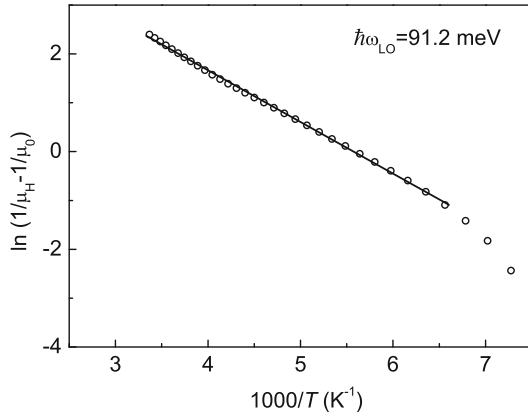
Fig. 9. The natural logarithm of the differential inverse mobility as a function of inverse temperature for an $Al_{0.83}In_{0.17}$N/AlN/GaN heterostructure. For symbols, refer to Fig. 1. The straight line is a least-squares fit to the experimental data.

Fig. 10. Room-temperature Raman spectrum for the $Al_{0.83}In_{0.17}$N/AlN/GaN heterostructure sample.

inverse mobility $(1/\mu_H - 1/\mu_0)$ can be approximated by[55–57]

$$\frac{1}{\mu_{LO}} = \frac{1}{\mu_H} - \frac{1}{\mu_0} = \frac{2m^*\alpha\omega_{LO}}{e}exp\left(-\frac{\hbar\omega_{LO}}{k_BT}\right), \quad (24)$$

where μ_0 is the low-temperature Hall mobility, which is independent of temperature, μ_H is the temperature-dependent Hall mobility measured at temperatures above approximately 90 K, α is the dimensionless polar constant, and ω_{LO} is the angular frequency of the optical phonon mode. Therefore, the LO phonon energy can be determined from a plot of the natural logarithm of $(1/\mu_H - 1/\mu_0)$ versus $1/T$. Figure 9 presents such a plot of the natural logarithm of $(1/\mu_H - 1/\mu_0)$ versus $1/T$. The LO phonon energy determined from the slope of the straight line, which is the best fit to the experimental data above approximately 170 K, is $\hbar\omega_{LO} = 91.2$ meV.

Figure 10 shows the room-temperature Raman spectrum for the $Al_{0.83}In_{0.17}$N/AlN/GaN heterostructure sample recorded in the grown-axis backscattering configuration $(z(xx)\bar{z})$. In our sample, GaN crystallizes in a wurtzite structure whose z-axis is perpendicular to the sapphire substrate plane. The space group is C_{6v}^4, and the A_1(LO) and E_2 modes are allowed in this configuration.[58] There is a sharp and strong peak at 575 cm^{-1}, known as the nonpolar high-frequency E_2 mode, which implies a strong correlation between Ga and N atoms on the c-plane.[58–60] The polar vibrations A_1(LO) observed at 738.5 cm^{-1} also correspond to a correlation between Ga and N atoms. Since the light penetration depth of 785 nm is longer than the thickness of the coated wafer on the sapphire substrate, the sapphire origin A_{1g} and E_g modes were observed at approximately 644 cm^{-1} and 754 cm^{-1}, respectively. The energy of LO phonons in GaN $(\hbar\omega_{LO} = 91.6$ meV$)$ is determined using $\hbar\omega_{LO} = \hbar c\bar{v}$,

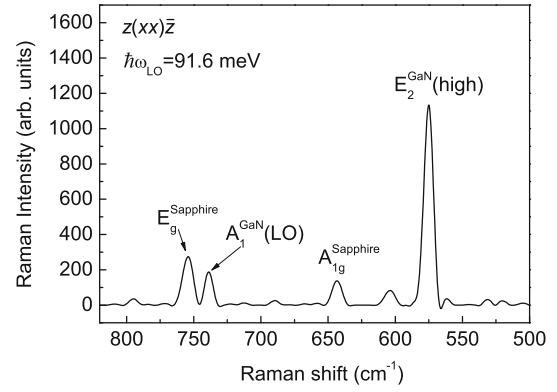where c is the speed of light and $\bar{v}$ is the wavenumber of the A_1(LO) mode. The value for $\hbar\omega_{LO}$ determined by this method is in good agreement with that $(\hbar\omega_{LO} = 91.2$ meV$)$ obtained from our present mobility measurements and that $(\hbar\omega_{LO} = 91.8$ meV$)$ reported in literature.[61,62]

We found that the ratio given in Eq. 23 is less than and equal to 1 using $k < k_F$ and our experimentally evaluated optical phonon energy. Therefore, it can be stated that the energy loss rate per electron for the $Al_{0.83}In_{0.17}$N/AlN/GaN heterostructure sample in the acoustic phonon regime is in agreement with the theoretical results. In addition, there is a small deviation between the experiment and theory at low electron temperature. This is probably because the ideal quantum-well approximation in the extreme quantum limit, which was used in the 2D power loss calculations, predicts an enhancement in the confined electron–acoustic phonon interaction, compared with the case in a real triangle quantum well with finite barriers in our $Al_{0.83}In_{0.17}$N/AlN/GaN heterostructure.[2,3,7,49] Furthermore, the existing 2D theories use the bulk phonon approximation, which requires consideration of the confinement and folding of the longitudinal and transverse acoustic modes.

The energy relaxation time (τ_E) for intrasubband processes can be obtained from the power loss measurements using[2]

$$P = \frac{<\hbar\omega>}{\tau_E}\frac{(k_BT_e - k_BT_L)}{k_BT_e}, \quad (25)$$

where $<\hbar\omega> = 2^{1/2}\hbar V_S k_F$ and $<\hbar\omega>$ is the acoustic phonon energy averaged over the Fermi surface. Figure 11 shows the energy relaxation time as a function of electron temperature for the $Al_{0.83}In_{0.17}$N/AlN/GaN heterostructure sample studied. Such large values of τ_E indicate that the energy loss mechanism in this temperature range is not very efficient and leads to rapid rise of the electron temperature when the input power is increased (Fig. 8). However, as can be seen in Fig. 11, the
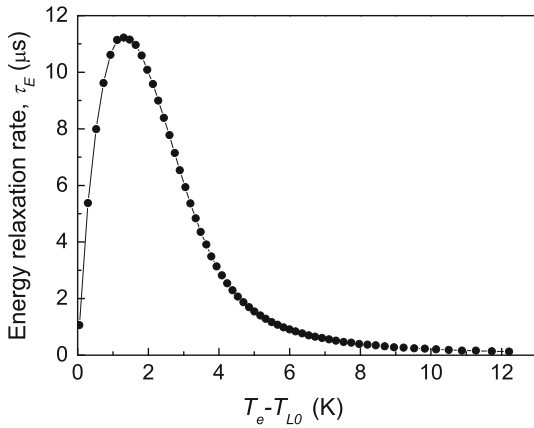
Fig. 11. Energy relaxation time (t_e) versus $T_e - T_{L0}$ for the $Al_{0.83}In_{0.17}N/AlN/GaN$ heterostructure. The solid curves through the experimental data points are intended as a guide for the eye.

energy relaxation due to acoustic phonons becomes faster at higher electron temperatures.

CONCLUSIONS

The carrier density (N_{2D}), effective mass (m^*), and quantum lifetime (τ_q) for electrons in an $Al_{0.83}In_{0.17}N/AlN/GaN$ heterostructure have been determined from the Shubnikov–de Haas (SdH) oscillations. The two-dimensional (2D) carrier density and the Fermi energy with respect to the subband energy ($E_F - E_1$) have been obtained from the periods of the SdH oscillations. The m^* and τ_q of electrons have been extracted from the temperature and magnetic field dependencies of the SdH amplitude, respectively. The results obtained for the transport-to-quantum lifetime ratios of the respective subbands indicate that the scattering of electrons by remote ionized impurities is on average forward displaced in momentum space.

The energy loss rates, in the acoustic phonon regime, of 2D electrons in an $Al_{0.83}In_{0.17}N/AlN/GaN$ heterostructure have also been investigated using SdH effect measurements. The experimental results were compared with the predictions of current theoretical models for power loss in semiconductors. The energy relaxation of electrons is due to acoustic phonon emission via unscreened piezoelectric interaction. In the low-temperature regime, the piezoelectric component is significantly greater than the deformation potential component of the 2D power loss, for electron temperatures lower than 14 K.

ACKNOWLEDGEMENTS

REFERENCES

1. H. Morkoc, *Handbook of Nitride Semiconductors and Devices, Vol. I–III*. (Weinheim: Wiley–VCH, 2008).
2. B.K. Ridley, *Rep. Prog. Phys.* 54, 169 (1991).
3. N. Balkan, H. Celik, A.J. Vickers, and M. Cankurtaran, *Phys. Rev. B* 52, 17210 (1995).
4. N. Balkan, *Hot Electrons in Semiconductors: Physics and Devices*. (Oxford: Clarendon, 1998).
5. P.J. Price, *J. Appl. Phys.* 53, 6863 (1982).
6. S.D. Sarma, J.K. Jain, and R. Jalabert, *Phys. Rev. B* 37, 6290 (1989).
7. Y. Okuyama and N. Tokuda, *Phys. Rev. B* 40, 9744 (1989).
8. H. Kahlert and G. Bauer, *Phys. Status Solidi B* 46, 535 (1971).
9. G. Bauer and H. Kahlert, *Phys. Rev. B* 5, 566 (1972).
10. M.C. Arikan, A. Straw, and N. Balkan, *J. Appl. Phys.* 74, 6261 (1993).
11. S. Mazzucato, M.C. Arikan, N. Balkan, B.K. Ridley, N. Zakhleniuk, R.J. Shealy, and B. Schaff, *Phys. B* 314, 55 (2002).
12. N. Balkan, M.C. Arikan, S. Gokten, V. Tilak, and B. Schaff, *J. Phys. Condens. Matter* 14, 3457 (2002).
13. A. Ilgaz, S. Gokten, R. Tulek, A. Teke, S. Ozcelik, and E. Ozbay, *Eur. Phys. J. Appl. Phys.* 55, 30102 (2011).
14. A. Matulionis, J. Liberis, E. Sermuksnis, J. Xei, J.H. Leach, M. Wu, and H. Morkoc, *Semicond. Sci. Technol.* 23, 075048 (2008).
15. A. Matulionis, *J. Phys. Condens. Matter* 21, 174203 (2009).
16. K.T. Tsen, J.G. Kiang, D.K. Ferry, and H. Morkoc, *Appl. Phys. Lett.* 89, 112111 (2006).
17. K.J. Lee, J.J. Harris, A.J. Kent, T. Wang, S. Sakai, D.K. Maude, and J.C. Portal, *Appl. Phys. Lett.* 78, 2893 (2001).
18. N.M. Stanton, A.J. Kent, S.A. Cavill, A.V. Akimov, K.J. Lee, J.H. Harris, T. Wang, and S. Sakai, *Phys. Status Solidi B* 228, 607 (2001).
19. C.E. Martinez, N.M. Stanton, A.J. Kent, M.L. Williams, I. Harrison, H. Tang, J.B. Webb, and J.A. Bardwell, *Semicond. Sci. Technol.* 21, 1580 (2006).
20. H. Cheng, N. Biyikli, J. Xie, C. Kurdak, and H. Morkoc, *J. Appl. Phys.* 106, 103702 (2009).
21. J. Xie, X. Ni, M. Wu, J.H. Leach, U. Ozgur, and H. Morkoc, *Appl. Phys. Lett.* 91, 132114 (2007).
22. R. Butte, J.-F. Carlin, E. Feltin, M. Gonschorek, S. Nicolay, G. Christmann, D. Simeonov, A. Castiglia, J. Dorsaz, H.J. Buemann, S.G. Baldassarri, H. von Hogersthal, A.J.D. Grundy, M. Mosca, C. Pinquier, M.A. Py, F. Demangeot, J. Frandon, P.G. Lagoudakis, J.J. Baumberg, and N. Grandjean, *J. Phys. D Appl. Phys.* 40 (2007).
23. A. Teke, S. Gokden, R. Tulek, J.H. Leach, Q. Fan, J. Xie, U. Ozgur, H. Morkoc, S.B. Lisesivdin, and E. Ozbay, *New J. Phys.* 11, 063031 (2009).
24. J. Shah, *Hot carriers in Semiconductors Physics and Applications*. (USA: Academic, 1992).
25. E. Tiras, M. Cankurtaran, H. Celik, and N. Balkan, *Phys. Rev. B* 64, 085301 (2001).
26. E. Tiras, N. Balkan, S. Ardali, M. Gunes, F. Fontaine, and A. Arnoult, *Philos. Mag.* 91, 628 (2011).
27. J. Shah, A. Pinczuk, H.L. Stormer, A.C. Gossard, and W. Wiegmann, *Appl. Phys. Lett.* 44, 322 (1984).
28. V. Karpus, *Fiz. Tekh. Poluprovodn.* 22, 439 (1988) [*Sov. Phys. Semicond.* 22, 268 (1988)].
29. A.M. Kreshchuk, M.Y. Martisov, T.A. Polyanskaya, I.G. Savel'ev, I.I. Saidashev, A.Y. Shik, and Y.V. Shmartsev, *Fiz. Tekh. Poluprovodn.* 22, 604 (1988) [*Sov. Phys. Semicond.* 22, 377 (1988)].
30. A.M. Kreshchuk, M.Y. Martisov, T.A. Polyanskaya, I.G. Savel'ev, I.I. Saidashev, A.Y. Shik, and Y.V. Shmartsev, *Solid State Commun.* 65, 1189 (1988).
31. P. Hawker, A.J. Kent, O.H. Hughes, and L.J. Challis, *Semicond. Sci. Technol.* 7, B29 (1992).
32. B.N. Murdin, W. Heiss, C.J.G.M. Langerak, S.-C. Lee, I. Galbraith, G. Strasser, E. Gornik, M. Helm, and C.R. Pidgeon, *Phys. Rev. B* 55, 5171 (1997).
33. T. Ando, *J. Phys. Soc. Jpn.* 37, 1233 (1974).
34. T. Ando, A.B. Fowler, and F. Stern, *Rev. Mod. Phys.* 54, 437 (1982).
35. E. Tiras, M. Cankurtaran, H. Celik, A. Boland-Thoms, and N. Balkan, *Superlattices Microstruct.* 29, 147 (2001).

36. P.K. Milsom and P.N. Butcher, *Semicond. Sci. Technol.* 1, 58 (1986).
37. M.P. Vaughan and B.K. Ridley, *Phys. Rev. B* 72, 075211 (2005).
38. H. Celik, M. Cankurtaran, N. Balkan, and A. Bayrakli, *Semicond. Sci. Technol.* 17, 18 (2002).
39. G. Weimann, *Festkorperprobleme Adv. Solid State Phys.* 26, 231 (1986).
40. S. Hiyamizu, J. Saito, K. Nanbu, and T. Ishikawa, *Jpn. J. Appl. Phys.* 22, L609 (1983).
41. E.E. Mendez, P.J. Price, and M. Heiblum, *Appl. Phys. Lett.* 45, 294 (1984).
42. L. Ardaravicius, M. Ramonas, J. Liberis, O. Kiprijanovic, A. Matulionis, J. Xie, M. Wu, J.H. Leach, H. Morkoc, *J. Appl. Phys.* 106, 073708 (2009).
43. R.A. Stradling and R.A. Wood, *J. Phys. C Solid State Phys.* 3, L94 (1970).
44. H. Celik, M. Cankurtaran, A. Bayrakli, E. Tiras, and N. Balkan, *Semicond. Sci. Technol.* 12, 389 (1997).
45. M. Cankurtaran, H. Celik, E. Tiras, A. Bayrakli, and N. Balkan, *Phys. Status Solidi B* 207, 139 (1998).
46. A.M. Kurakin, S.A. Vitusevich, S.V. Danylyuk, H. Hardtdegen, N. Klein, Z. Bougrioua, A.V. Naumov, and A.E. Belyaev, *J. Appl. Phys.* 105, 073703 (2009).
47. I. Vurgaftman, J.R. Meyer, and L.R. Ram-Mohan, *J. Appl. Phys.* 89, 5815 (2001).
48. M.J. Kane, N. Apsley, D.A. Anderson, L.L. Taylor, and T. Kerr, *J. Phys. C Solid State Phys.* 18, 5629 (1985).
49. M. Cankurtaran, H. Celik, and N. Balkan, *Phys. Status Solidi B* 229, 1191 (2002).
50. W.J. Fan and S.F. Yoon, *J. Appl. Phys.* 90, 843 (2001).
51. S. Adachi, *Properties of Semiconductor Alloys: Group IV, III-V and II-VI Semiconductors*, 1st edn. (UK: Wiley, 2009).
52. A.D. Bykhovski, V.V. Kaminski, M.S. Shur, Q.C. Chen, and M.A. Khan, *Appl. Phys. Lett.* 68, 818 (1996).
53. P. Tripathi and B.K. Ridley, *Phys. Rev. B* 66, 195301 (2002).
54. C. Bulutay, B.K. Ridley, and N.A. Zakhleniuk, *Phys. Rev. B* 68, 115205 (2003).
55. K. Seeger, *Semiconductor Physics—An Introduction*, 6th ed. (New York: Springer-Verlag, 1997).
56. S. Altinoz, E. Tiras, A. Bayrakli, H. Celik, M. Cankurtaran, and N. Balkan, *Phys. Status Solidi A* 182, 717 (2000).
57. E. Tiras, M. Gunes, N. Balkan, and W.J. Schaff, *Phys. Status Solidi B* 247, 189 (2010).
58. T. Azuhata, T. Sota, K. Suzuki, and S. Nakamura, *J. Phys. Condens. Matter* 7, L129 (1995).
59. T. Kozawa, T. Kachi, H. Kano, Y. Taga, and M. Hashimoto, *J. Appl. Phys.* 75, 1098 (1994).
60. M. Ramsteiner, O. Brandt, and K.H. Ploog, *Phys. Rev. B* 58, 1118 (1998).
61. V.Yu. Davydov, Yu.E. Kitayev, I.N. Goncharuk, A.N. Smirnov, J. Graul, O. Semchinova, D. Uffmann, M.B. Smirnov, A.P. Mirgorodsky, and R.A. Evarestov, *Phys. Rev. B* 58, 12899 (1998).
62. M. Kuball, *Surf. Interface Anal.* 31, 987 (2001).